An Accurate and Efficient Empirical Approach for Calculating the Dielectric Self-Energy and Ion−Ion Pair Potential in Continuum Models of Biological Ion Channels

Mary Hongying Cheng and Rob D. Coalson*

Department of Chemistry, University of Pittsburgh, Pittsburgh, Pennsylvania 15260

Received: June 14, 2004; In Final Form: August 24, 2004

This paper presents empirical formulas for calculating the dielectric self-energy and ion−ion pair interactions in cylindrical ion channels. The proposed approach can be extended to more complex channel structures, for example, (i) a "straight" channel with variable radius and (ii) a "curved" channel with constant radius. For calibration purposes, we compare results obtained based on the approximate effective potentials developed herein to exact electrostatic calculations obtained via the algorithm of Graf et al.:[1,2] the agreement is satisfactory. A dynamic lattice Monte Carlo (DLMC) technique is used to further assess the accuracy and efficiency of the proposed empirical potentials. The concentration profiles and current−voltage curves produced with our simple empirical energy formulas are in excellent agreement with numerical results obtained using the algorithm of Graf et al., which calculates all relevant electrostatic forces exactly. The use of effective ion−ion potentials greatly reduces the computer memory required to perform DLMC ion permeation simulations in dielectrically inhomogeneous environments, thus enabling treatment of larger systems than can be handled by numerically exact techniques.

I. Introduction

Ion channels promote the transport of selected ions across cell membranes and thus contribute to physiological function in many essential ways. The cylindrical channel is a useful primitive model for many biological ion channels, e.g., the family of gramicidin channels.[3−5] Despite the relative simplicity of this channel structure, a complete understanding of the ion permeation mechanisms associated with it is still lacking. While several semimicroscopic treatments of the protein/membrane/water system have produced permeation barriers that are qualitatively consistent with experimentally measured ion conductivities,[6,7] all-atom molecular dynamics simulations of gramicidin A typically yield unphysically high energy barriers to ionic transport in the range of $10k_BT$ to $30k_BT$.[8−10] Even very recent high-level all-atom molecular dynamics calculations imply a conductance 5 orders of magnitude less than the experimentally measured value.[8]

Recent progress in determining the 3D structures of biological ion channels[11−13] has greatly facilitated theoretical/numerical modeling of these systems. Although experimental studies have provided a wealth of structural information, a fully atomistic simulation of ion permeation is intractable on large time and length scales. Coarse-grained models sacrifice some realism, but by virtue of their relative simplicity make it possible to calculate ion permeation kinetics on currently available computing platforms. Among such models, Poisson−Nernst−Planck theory,[14−17] Brownian dynamics,[18−22] and the dynamic lattice Monte Carlo technique[1,2] have been extensively applied to investigate ion permeation and related processes.

Electrostatic effects clearly play a major role in determining ion selectivity and ion permeation. When an ion moves through a dielectrically inhomogeneous environment, it experiences a force due to the spatial variation of the dielectric self-energy (DSE). In particular, the DSE of an ion increases when it moves from a bulk solution characterized by a high dielectric constant, such as water, to an aqueous pore region surrounded by a low dielectric medium such as protein and membrane (comprised of a lipid bilayer). The cell membrane provides a significant energy barrier to the passage of the ions. The first quantitive estimation of the energy barrier for ion transport through the cell membrane was provided by Parsegian.[23] For the case where the channel radius R_p is much smaller than its length L (i.e., an infinite cylindrical channel), the self-energy for an ion with charge q residing at the center of the channel is

$$\phi^{\text{self}} = \frac{q^2}{2\epsilon_w a} + \frac{q^2}{\epsilon_m R_p} P\left(\frac{\epsilon_m}{\epsilon_w}\right) \tag{1}$$

where a is the radius of the ion, ϵ_m and ϵ_w are the dielectric constants inside the membrane region and the aqueous pore, respectively, and $P(\epsilon_m/\epsilon_w)$ is a dimensionless function of the dielectric constant ratio [cf. Parsegian[23] for details]. The first term on the right-hand side of eq 1 represents the self-energy of an ion in an infinite homogeneous medium and the second term adds to this an additional energy barrier due to dielectric inhomogeneity. Subsequently, Levitt[4] and Jordan[5] formulated an approach based on the method of images and numerically evaluated the energy barrier for a cylindrical channel of finite length.

The present work seeks to develop an accurate and efficient numerical way to estimate ion−ion interactions in a dielectrically heterogeneous medium, especially one provided by a biological ion channel/membrane system. We shall consider throughout a model in which all parts of the system except the permeant ions are treated as dielectric continua. Water is treated as a dielectric medium (characterized by dielectric constant ϵ_w) through which the ions can move. The protein and membrane are treated as a static, impermeable dielectric medium characterized by a single dielectric constant ϵ_m. Of course, this is an idealization of the behavior of the full microscopic system, in which water, the protein, and the lipid bilayer membrane participate in atomistic

10.1021/jp047438w CCC: $30.25
Published on Web 12/13/2004

detail. There are many difficulties inherent in the implied reduction from fully atomistic to highly coarse grained levels of description. For example, the dielectric constant of water in the narrow pore may not be equal to its value in the bulk solvent: indeed, the former may be ill defined, due to the small number of water molecules in the pore at any instant of time. Furthermore, the protein and membrane are not static objects, but rather they fluctuate on picosecond and longer time scales, while an ion permeation event typically takes nanoseconds. Even if no major structural reorganization occurs during the course of ion permeation, these membrane/protein fluctuations influence the energetics of ion permeation in several ways. For example, they contribute to the polarizability of the membrane/protein medium,[6] and pore lining groups (e.g., carbonyl groups in gramidin A) form directed electrostatic "bonds" with ions in the channel.[7] Such effects are difficult to inscribe into a continuum model of the solvent and the membrane/protein. Nevertheless, some progress has been made in this direction,[6−7] i.e., in feeding up information extracted from microscopic or semimicroscopic models to refine the parameters that enter into coarse-grained continuum models. This provides further motivation (in addition to that of conceptual simplicity) for careful studies of the properties of the basic continuum model of an ion channel and its immediate environment.

This paper is organized as follows: In Section II we briefly review the electrostatic background needed in later sections. In Section III, we present empirical expressions for approximating the dielectric contribution to the self-energy and the ion−ion interactions in cylindrical channels. Our empirical formulas are then applied to channels with more complex structures, namely, (i) a "straight" channel with variable channel radius along the permeation direction and (ii) a "curved" channel with fixed pore radius. The accuracy of these formulas is ascertained by comparison with exact electrostatic calculations based on the algorithm of Graf, Nitzan, Kurnikova ,and Coalson,[1] subsequently to be referred to as GNKC. (A recent application of the GNKC algorithm may be found in ref 2.) In Section IV, dynamic lattice Monte Carlo (DLMC) simulations of ion permeation are used to further calibrate the performance of our approach. The ion−ion pair interactions are calculated three different ways via (i) a Coulombic potential corresponding to a uniform dielectric medium characterized by static dielectric constant $\epsilon_w = 80$, (ii) the empirical formulas proposed in this paper, and (iii) the numerically exact approach developed by GNKC. Concentration profiles and the current−voltage curves obtained with each of these ion−ion interaction potentials are compared for several channel geometries. Conclusions are then presented in Section V.

II. Numerical Methods

Consider a cylindrical channel inserted into a membrane slab of dielectric constant ϵ_m such that it is oriented normal to the slab faces. The length of the channel is L and the radius of the aqueous pore is R_p. The membrane/channel system is in contact with a water bath on either side of the membrane slab (cf. Figure 1). For simplicity, the dielectric constant inside the aqueous pore (channel) is assumed to be the same as that in the bulk water bath, ϵ_w.

Numerical Solution Based on the Method of Images. As noted in the Introduction, some time ago Levitt and Jordan approximately evaluated the DSE for inserting an ion into a cylindrical channel. On the basis of his analysis, Jordan offered the following empirical formula for the DSE of a monovalent ion at the midpoint along a channel of length L and radius R_p (relative to its value in the bulk solution outside of the channel):[5]

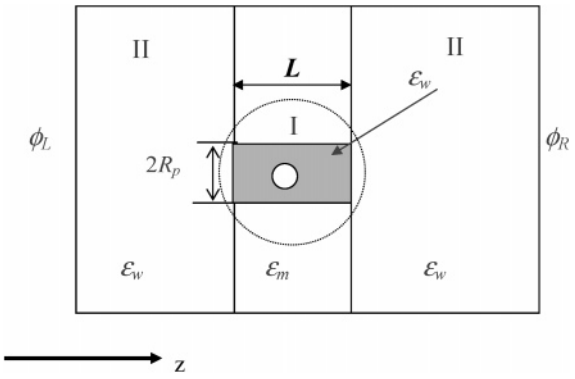

Figure 1. Cross section of the system under investigation. The cylindrical channel (shaded region) is characterized by a length L and radius R_p. The ion (in the channel) is assumed to be sphere of radius a. See the text for further details.

$$\phi(\Delta) = \phi_\infty(1 - \exp(-b\Delta)) \tag{2}$$

where Δ is the ratio of the channel length to the channel diameter, i.e., $\Delta = L/2R_p$; furthermore, the parameter $b = 0.131$ when $\epsilon_w/\epsilon_m = 40$, and ϕ_∞ is the DSE of a monovalent ion at the center of an infinitely long cylindrical channel (again, relative to its value in the bulk solution), as deduced earlier by Parsegian:[23]

$$\phi_\infty = \frac{28.36}{R_p}\,(\text{kcal/mol}) = \frac{47.93}{R_p}(k_B T) \tag{3}$$

with R_p measured in Å, k_B the Boltzmann constant, and T the absolute temperature (again, for the case that $\epsilon_w/\epsilon_m = 40$ and $\epsilon_m = 2$). We take $T = 298$ K throughout this paper. Comparison with numerically exact calculations performed by using the methodology of GNKC reveals that eq 2 is rather accurate (vide infra). The analyses of Parsegian, Levitt, and Jordan treat the ion as a point source when calculating ϕ_∞ and $\phi(\Delta)$, and thus ignore electrostatic effects associated with its finite radius, a. As discussed below, we find numerically that such effects are indeed negligibly small.

Numerical Approach of GNKC. GNKC proposed a numerical approach for obtaining the self-energy of an ion in an arbitrary inhomogeneous dielectric medium,[1] which we follow here. The potential generated by an ion with +1 charge is taken to be a truncated Coulomb potential:

$$\phi^{\text{coul}}(r) = \begin{cases} 1/a - 1/r_c & r < a \\ 1/r - 1/r_c & a < r < r_c \\ 0 & r_c < r \end{cases} \tag{4}$$

where r is the distance from the ion center, a is the ion radius, and r_c is an imposed cutoff distance. The charge distribution of the ion is obtained as a lattice charge distribution ρ_k^{coul}, which is constructed by operating with the lattice Laplacian ∇^2 on the truncated Coulombic potential $\phi^{\text{coul}}(r)$ generated by a unit charge at the lattice position k. (The result of operating on $\phi^{\text{coul}}(r)$ with the lattice Laplacian is divided by -4π to give ρ_k^{coul}.) The actual electrical potential associated with this lattice charge distribution and the full spatially inhomogeneous dielectric profile is then obtained by solving the following Poisson equation:

$$\nabla\epsilon\nabla\phi_k = -4\pi\rho_k^{\text{coul}} \tag{5}$$

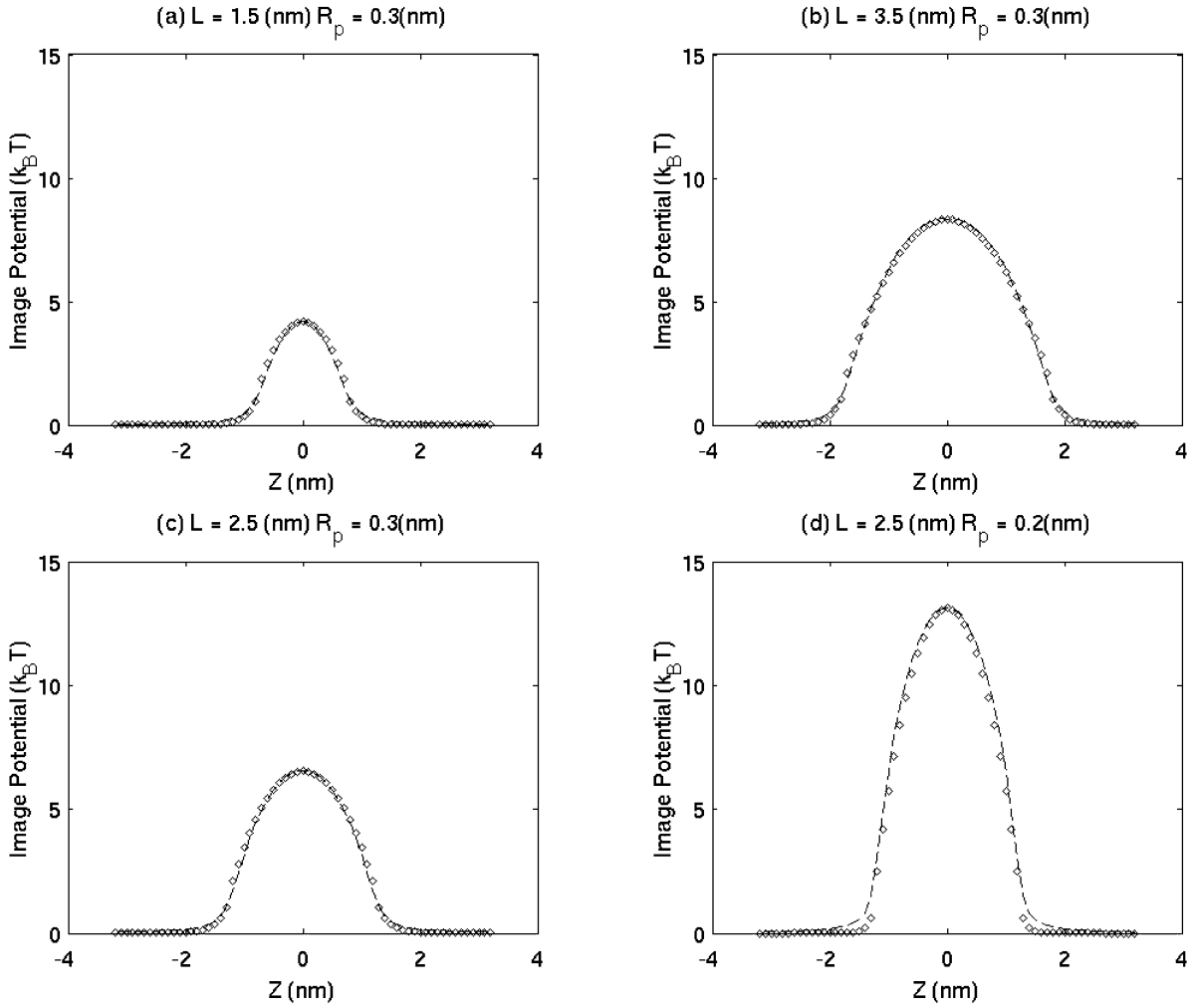

Figure 2. The dielectric contribution to the self-energy profile along the centerline of a cylindrical channel for various channel geometries: (a) $L = 1.5$ nm and $R_p = 0.3$ nm, (b) $L = 3.5$ nm and $R_p = 0.3$ nm, (c) $L = 2.5$ nm and $R_p = 0.3$ nm, (d) $L = 2.5$ nm and $R_p = 0.2$ nm. [Here and throughout the ion is monovalent.] In each plot, the dashed line represents the result with the GNKC procedure while the diamond represents the result based on eqs 10 and 11 (with $\phi^{diel}(z_c,0)$ and $\phi^{diel}(z_{in},0)$ obtained numerically via the GNKC procedure).

In the present work Coulomb boundary conditions[24] are applied in solving eq 5 for the purpose of computing the self-energy of an ion. Namely, on the boundary faces perpendicular to $\hat{z}$ (cf. Figure 1), we set the potential as $\phi^{coul}(r)/\epsilon_w$, i.e., based on a positive unit point charge source at position r_k corresponding to lattice point k (somewhere in the aqueous medium) in a uniform dielectric medium characterized by the solvent dielectric constant. This represents the asymptotic dependence of the electric potential in the dielectrically inhomogeneous system of interest (far away from the region characterized by ϵ_m). The self-energy of this singly charged ion at point k is then given by:

$$\phi_k^{self} = \frac{1}{2}\phi_{k\leftarrow k} \tag{6}$$

where $\phi_{k\leftarrow k}$ is the electric potential ϕ_k at lattice point k. The self-energy of an ion of charge q placed at lattice position k is $q^2\phi_k^{self}$.

Numerical solution of the 3D Poisson equation is accomplished via a standard finite difference relaxation algorithm.[1,25] Parameter details are specified below. We have compared our numerical results for the DSE at the channel center with those obtained by Levitt[4] and Jordan.[5] All these results are within each other by $0.1k_BT$ for $\Delta \leq 6.0$. For $\Delta > 6.0$, our results are closer to Jordan's calculation than to Levitt's. For example, for $L = 5$ nm and $R_p = 0.2$ nm, the dielectric contribution to the self-energy (defined precisely in eq 8 below) equals $17.2k_BT$, $18.6k_BT$, and $18.3k_BT$, based on Levitt, Jordan, and the present numerical study, respectively.

III. Empirical Potentials and Their Parametrization

Dielectric Contribution to the Self-Energy. In a uniform dielectric medium ϵ_1, the self-energy of an ion of charge q and radius a is essentially its Born charging energy:[4]

$$\phi^{self} = \int_0^q \phi_s(e)\, de = \frac{q^2}{2\epsilon_1 a} \tag{7}$$

where ϕ_s is the potential at the surface of the ion, and q is the total charge of the ion. When the ion is placed in an inhomogeneous medium, specifically, in a cylindrical channel of dielectric constant ϵ_1 surrounded by material characterized by dielectric ϵ_2, surface charge is induced at the dielectric boundary. Consequently, the self-energy consists of two parts:

$$\phi^{self} = \frac{q^2}{2\epsilon_1 a} + \phi^{diel} \tag{8}$$

where ϕ^{diel} is the dielectric contribution to the self-energy. [Note: ϕ^{diel} is the quantity that was evaluated approximately by

Parsegian and Jordan in eqs 2 and 3 above.] For $\epsilon_2 > \epsilon_1$, one finds $\phi^{\text{diel}} < 0$, corresponding to a favorable charging process, while for $\epsilon_2 < \epsilon_1$ one finds $\phi^{\text{diel}} > 0$, corresponding to an unfavorable dielectric self-energy (DSE) penalty. We have found in our numerical studies that the ion radius has an insignificant effect on ϕ^{diel}. For example, if the test ion does not overlap with the channel wall, the difference in the value of ϕ^{diel} obtained (with $\epsilon_1 = 80$, $\epsilon_2 = 2$, $L = 25$ Å, and $R_p = 3$ Å) is within 0.2% for ion sizes of 0.5, 1.0, and 2.0 Å. Following an approach similar to that of Burykin et al.,[22] the dielectric contribution to the self-energy can be approximated as:

$$\phi^{\text{diel}}(z,r) = \phi^{\text{diel}}(z,0) + \Delta\phi^{\text{diel}}(z,0\rightarrow r) \qquad (9)$$

The first term on the right-hand side is the dielectric contribution to the self-energy along the channel centerline ($r = 0$), and the second term represents the energy change associated with moving the ion transverse to the channel axis, i.e., along the channel radial direction. $\phi^{\text{diel}}(z,0)$ in a cylindrical channel can be parametrized in the following way:

inside the pore: $\phi^{\text{diel}}(z,0) =$

$$\phi^{\text{diel}}(z_c,0) + [\phi^{\text{diel}}(z_{in},0) - \phi^{\text{diel}}(z_c,0)]\left(\frac{z - z_c}{L/2}\right)^2 \qquad (10)$$

in the water bath: $\phi^{\text{diel}}(z,0) =$

$$\phi^{\text{diel}}(z_{in},0)\exp(-|z - z_{in}|/r_0) \qquad (11)$$

where $\phi^{\text{diel}}(z_c,0)$ is the dielectric contribution to the self-energy at the channel center ($z = z_c$). For a cylindrical channel, $\phi^{\text{diel}}(z_c,0)$ is well studied and empirical formulas, e.g., eq 2, are available. $\phi^{\text{diel}}(z_{in},0)$ is the dielectric contribution to the self-energy at the inlet of the channel, which can be obtained numerically. Furthermore, in eqs 10 and 11, $|z - z_{in}|$ is the distance from the channel entrance, $|z - z_c|$ is the distance from the channel center, and r_0 is a characteristic distance: in the present work we adopt the specific value $r_0 = 2.0$ Å. For the important case of a monovalent ion (which we shall focus on throughout this exposition) and the dielectric constant profile $\epsilon_w = 80$, $\epsilon_m = 2$ (which shall be utilized throughout, except where explicitly noted otherwise), Figure 2 compares an exact numerical calculation with the empirical formula for the dielectric contribution to the self-energy described above for a range of channel dimensions. The agreement is satisfactory. [Note: Most of the numerical calculations performed in this section (specifically, those presented in Figures 2, 5−7, 9, and 10) were performed on a $(135)^3$ lattice, with a grid spacing $h = 1$ Å, and $a = 1.0$ Å, $r_c = 64$ Å.]

The second term in eq 9 represents (for $\epsilon_1 > \epsilon_2$) the repulsive force due to the DSE penalty when the ion is moved off the centerline in the radial direction (i.e., toward the low dielectric channel/membrane medium). For an ion residing in the water bath, $\Delta\phi^{\text{diel}}(z,0\rightarrow r)$ is expected to be roughly zero even when the ion is near the surface of the membrane. For an ion residing inside the channel, this term can be represented by a power series in r^n with $n = 2, 4, 6, \ldots$. We found in our numerical studies that $\Delta\phi^{\text{diel}}(z,0\rightarrow r)$ increases as ca. r^2 near the center ($r = 0$) and as ca. r^{12} when the ion is close to the channel wall ($r = R_p$). Hence it is well described by an equation of the form:

$$\Delta\phi^{\text{diel}}(z,0\rightarrow r) = A(r/R_p)^2 + B(r/R_p)^{12} \qquad (12)$$

where A and B are positive constants. Specifically, the sum $A + B$ represents the energy barrier due to the induced polarization charge when an ion at position z along the channel axis is moved from the channel centerline to the channel wall. This energy barrier depends in general on the channel geometry, but it has a weak dependence on position along the channel z axis unless the ion is very close to the channel entrance. Figure 3 shows the radial energy barrier as a function of the position of the ion along the channel z axis direction. This energy barrier reaches a maximum value 2.5 Å inside the channel entrance. Figure 4 compares the radial variation of the dielectric energy barrier at $z = 0$ (channel center) for several channel radii. In this plot, the length of the channel is fixed at 2.5 nm and the channel radius ranges from $R_p = 0.2$ to 0.5 nm. The agreement is satisfactory with parameter values $A = 3.0k_BT$ and $B = 16.0k_BT$. (Note that due to the rapid variation of the DSE in the radial direction, we used a finer grid with $h = 0.5$ Å to calculate the results shown in Figures 3 and 4; again, the grid dimensions are $(135)^3$, and $a = 0.5$ Å, $r_c = 32$ Å.)

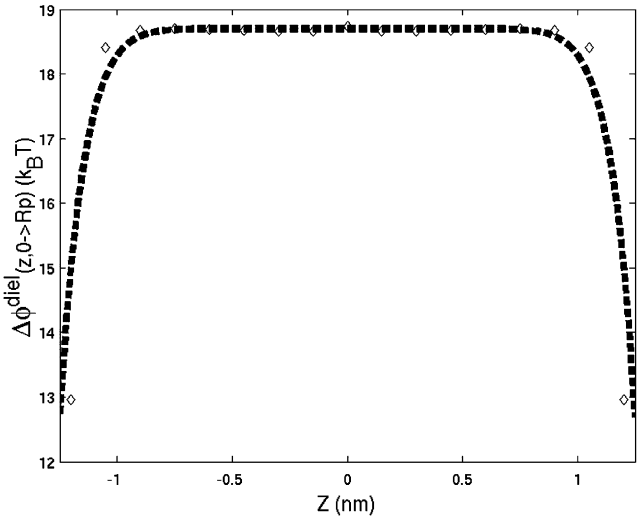

Figure 3. The radial DSE barrier along the channel direction z when an ion moves from $r = 0$ to R_p for the case that $L = 2.5$ nm and $R_p = 0.3$ nm. Open diamonds are data points obtained via the GNKC procedure; the dashed line is a least-squares fit to this data.

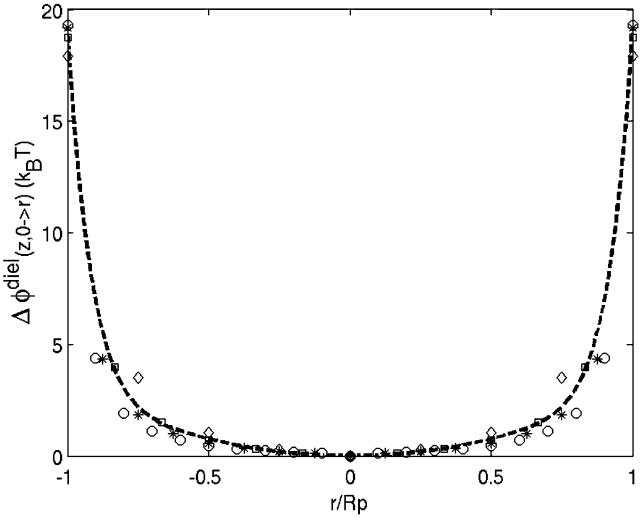

Figure 4. Radial variation of the DSE barrier at the centerline $z = 0$. The length of the channel is fixed at 2.5 nm and the channel radius ranges from $r = 0.2$ to 0.5 nm. The dashed line shows the result of eq 12 with $A = 3.0(k_BT)$ and $B = 16.0(k_BT)$. The symbols represent data points obtained via the GNKC procedure: diamonds for $R_p = 0.2$ nm, squares for $R_p = 0.3$ nm, stars for $R_p = 0.4$ nm, and circles for $R_p = 0.5$ nm.

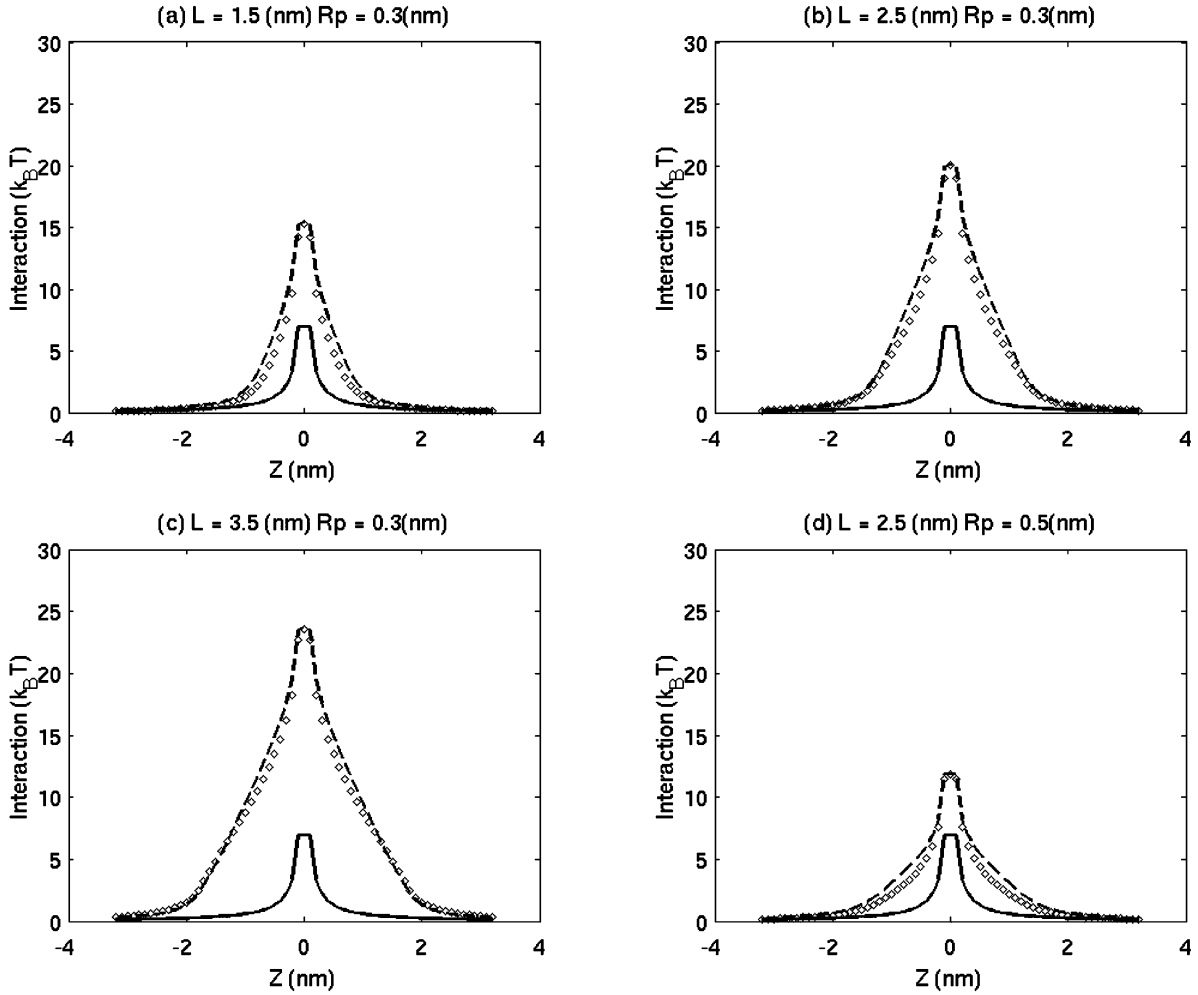

Figure 5. Ion−ion interaction energy between two monovalent ions of the same sign in channels having the following dimensions: (a) $L = 1.5$ nm and $R_p = 0.3$ nm, (b) $L = 2.5$ nm and $R_p = 0.3$ nm, (c) $L = 3.5$ nm and $R_p = 0.3$ nm, and (d) $L = 2.5$ nm and $R_p = 0.5$ nm. One ion is fixed at the channel center while a second ion is moved along the channel centerline. In each plot, the dashed line is the numerical evaluation using the GNKC procedure; diamonds show results of the empirical formula based on eq 16 with $c = 2.0$, and the solid line shows the Coulombic interaction in a uniform medium with ϵ_w.

Effective Ion−Ion Pair Potential. The net ion−ion interaction inside a protein channel depends on several complicated factors. For example, (1) screening due to the counterions in the water bath may give rise to variation in the dielectric constant in the immediate neighborhood of the charged ions[26] and (2) the polarization charge on the protein surface can affect the ion−ion interaction.[4] Warshel et al.[27] have suggested that the ion−ion pair potential inside a protein can be approximated as:

$$\phi_{ij}^{\text{int}} = \frac{q_i q_j}{r_{ij}\epsilon_{ij}} \tag{13}$$

$$\epsilon_{ij} = \epsilon_{\text{eff}} = 1 + \epsilon'(1 - \exp(-\mu r_{ij})) \tag{14}$$

where r_{ij} is the distance between the two ions i and j. Here ϵ_{ij} is a position-dependent effective dielectric constant for the ion−ion interaction; ϵ' and μ are constants, namely, $\epsilon' = 60$ and $\mu = 0.1$ Å^{-1}.

In the numerical approach of GNKC, the ion−ion pair interaction energy ϕ^{int} is calculated as the sum of two terms, namely, (1) a Coulombic interaction corresponding to a dielectrically uniform medium characterized by dielectric constant ϵ_w and (2) a dielectric contribution due to the inhomogeneous dielectric boundary between water and membrane/protein regions:

$$\phi_{ij}^{\text{int}} = q_i q_j \frac{\phi^{\text{coul}}(r_{ij})}{\epsilon_w} + q_i q_j \phi_{ij}^{\text{diel}} \tag{15}$$

ϕ_{ij}^{diel} is calculated by solving Poisson's equation twice with the imposed potential boundary $\phi_L = \phi_R = 0$: once for an ion in a uniform medium with $\epsilon = \epsilon_w$ and once for the same ion in the actual (nonuniform) dielectric field. The difference between these gives the relative dielectric contribution to the ion−ion interaction. This difference excludes the bare ion−ion interaction, which has been included as the first term of eq 15, and leaves only the contribution due to the dielectric inhomogeneity. The unphysical image contribution associated with the imposed boundary potential is also canceled in the difference.[1] For a given (lattice) position of the ion i_0 in the computational procedure just sketched, the quantity $\phi_{i_0 j}^{\text{diel}}$ is determined for all lattice points j. Clearly, this procedure must be repeated for each accessible ion position i_0 to generate the complete pair-potential ϕ_{ij}^{diel}. Note that ϕ_{ij}^{diel} is independent of the sign or magnitude of the two charges involved.

Calculation of this dielectric contribution on the fly is computationally inefficient because solving Poisson's equation is time consuming. The approach of GNKC uses lookup tables to store precalculated values of ϕ_{ij}^{diel}. Even so, the computation is expensive. For one ion at position i, extensive computer memory is required to store the values of ϕ_{ij}^{diel} for any arbitrary

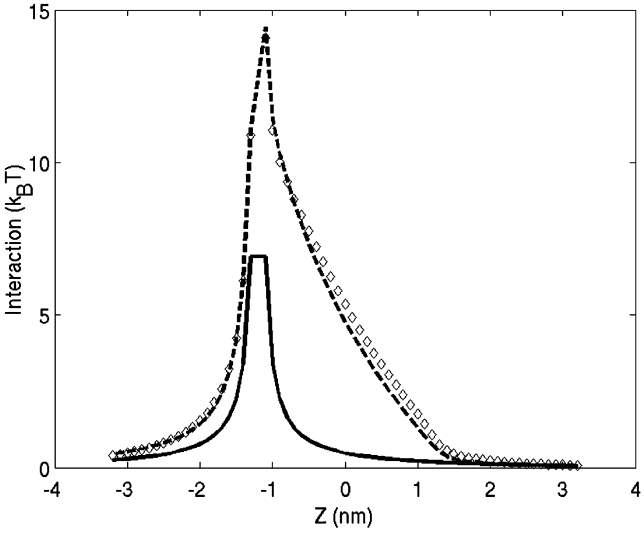

Figure 6. Ion−ion interactions in a cylindrical channel with $L = 2.5$ nm and $R_p = 0.2$ nm. One ion is fixed at the channel inlet, $z = -12$ Å, while a second ion is moved along the channel centerline. The dashed line indicates the results of numerical evaluation based on the GNKC procedure; the diamond points are the results of the empirical formula eq 16 with $c = 2.0$; the solid line plots the Coulombic interaction in a uniform medium with ϵ_w.

position in the system. In the present study, we have found that ϕ_{ij}^{diel} can be obtained to satisfactory accuracy from the following simple empirical formula:

$$\phi_{ij}^{\text{diel}} = 2\sqrt{\phi_{i\leftarrow i}^{\text{diel}}\,\phi_{j\leftarrow j}^{\text{diel}}}\,\exp(-cr_{ij}/L) \tag{16}$$

where $\phi_{i\leftarrow i}^{\text{diel}}$ is the dielectric contribution to the self-energy at point i with a unit (proton) charge (calculated exactly, or approximated via eqs 9−12), and c is a dimensionless parameter depending on the channel geometry, i.e., Δ. (With this convention for the units of ϕ_{ij}^{diel}, the charges q_i, q_j which scale the second term on the right-hand side of eq 15 should be specified as multiples of the proton charge.) Notice that the approximate formula for ϕ_{ij}^{diel} prescribed in eq 16 is independent of the magnitude or sign of the charge on ions i or j, consistent with the properties of the exact solution described above.

We calculated the ion pair interaction using eq 16 by placing one monovalent ion at the center of the cylindrical channel and moving a second ion of the same charge from the bulk solution into the channel. For $2.0 < \Delta \leq 6.5$ (the channel dimensions of Gramicidin A lie in this range), we found that the exact numerical results for ϕ_{ij}^{diel} could be well accounted for using the constant value $c = 2.0$. Figure 5 compares the ion−ion interactions calculated with different computational strategies and several values of L and R_p. The results based on the empirical formula eq 16 are consistent with those obtained based on the GNKC algorithm. We found that the value $c = 2.0$ can also be employed to successfully calculate the interactions between two ions at arbitrary positions along the centerline, instead of fixing one ion at the channel center. For example, in Figure 6 results are presented for the case where one ion is placed at the entrance of the channel.

Note that eq 16 for the dielectric contribution to the ion−ion interaction calculated is regarded here as empirical. When Δ increases beyond the upper limit noted above, it becomes necessary to change the value of c in order for eq 16 to generate accurate results. For example, for $L = 5$ nm and $R_p = 0.2$ nm, i.e., $\Delta = 12.5$, the value $c = 3.0$ gives the best results.

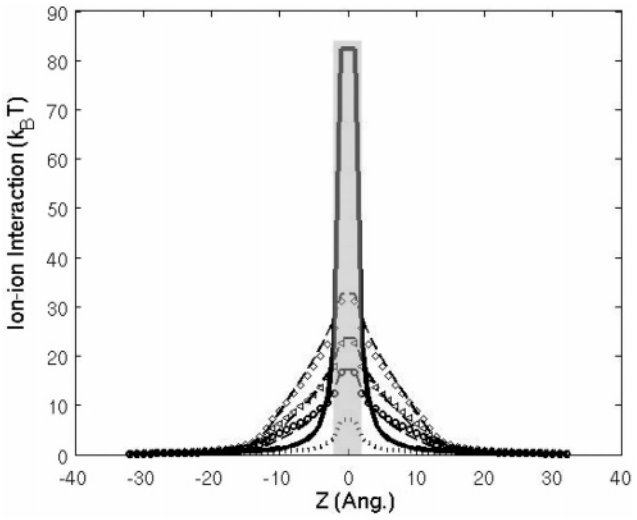

Figure 7. Ion−ion interactions in a cylindrical channel with $L = 2.5$ nm and $R_p = 0.2$ nm. One ion is fixed at the channel center, while a second ion is moved along the channel centerline in the z direction in increments of 0.1 nm. The dashed line presents the result of numerical simulation based on the GNKC algorithm with $\epsilon_m = 2$ and the diamonds show results of the empirical formula eq 16 with $c = 2.0$ and $\epsilon_m = 2$; the dot dashed line presents the result of numerical simulation based on the GNKC algorithm with $\epsilon_m = 5$ and the triangles show results of the empirical formula eq 16 with $c = 2.0$ and $\epsilon_m = 5$; the lower dashed line presents the result of numerical simulation based on the GNKC algorithm with $\epsilon_m = 10$ and the circles show the results of empirical formula eq 16 with $c = 2.0$ and $\epsilon_m = 10$; the dotted line plots the Coulombic interaction in a uniform medium with ϵ_w; the solid line shows results based on eqs 13 and 14 (Warshel et al.). The shaded region ($r_{ij} < 2$ Å) is not accessible due to the finite size of the ions.

As noted above, it has been suggested previously that ion−ion interactions ϕ_{ij} can be described by a Coulomb potential with position-dependent effective dielectric constant ϵ_{eff}, which is thus determined via:[27−29]

$$\epsilon_{\text{eff}} = q_i q_j / r_{ij}\phi_{ij} \tag{17}$$

For the case where the dielectric inhomegeneity (or equivalently the induced surface charge) contributes to the interaction, the origin of the dielectric contribution to the ion−ion interaction is complicated and depends strongly on the ion positions relative to the dielectric boundary. An explicit representation of ϵ_{eff} as a function of r_{ij}, e.g., eq 14, may not accurately account for the dielectric contribution in biological ion channels. The empirical formula eq 16 on the other hand represents the dielectric contribution faithfully because $\phi_{i\leftarrow i}^{\text{diel}}$ and $\phi_{j\leftarrow j}^{\text{diel}}$ contain local information concerning the polarization contribution (i.e., due to the induction of charge on a dielectric boundary when an ion approaches it). We should stress that the position-dependent dielectric constant model advanced by Warshel and co-workers[27,30,31] was not optimized for studying the problem of ion energetics in a continuum dielectric model of the protein/membrane/water system, but rather to account for ion−ion interactions (usually between charged acidic amino acid side groups rather than permeant ions in a channel) obtained from more sophisticated, and presumably more realistic, semimicroscopic models of protein/solvent systems. Such models predict that the effective protein dielectric constant is different for single-ion properties such as the DSE than it is for ion−ion interactions: higher values of ϵ_m, typically in the range of 5−10, are imputed for the latter.

Figure 7 compares the ion−ion interaction obtained by using four different approaches: (i) GNKC,[1] (ii) Warshel et al.,[27] (iii)

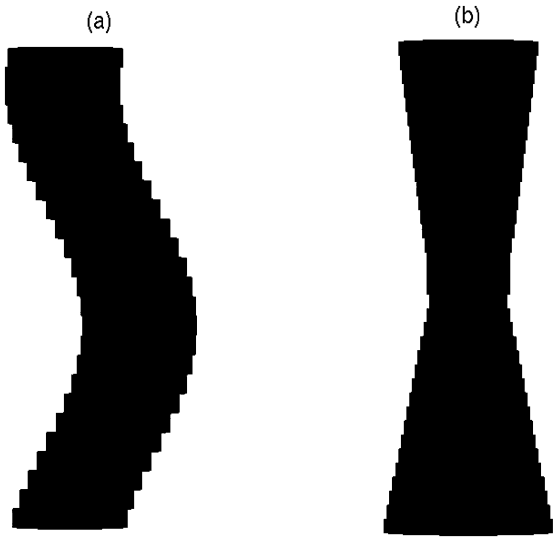

Figure 8. Geometries of two noncylindrical channels: (a) a channel with a curved centerline. The centerline (x_c^i, y_c^i) varied as $x_c^i = 2 \sin(2\pi i\Delta x/L)$ and $y_c^i = 2 \cos(2\pi i\Delta y/L)$, with i being the lattice site index along the channel direction, starting from 0 at one channel entrance. Δx and Δy are the lattice size in the x and y directions; $R_p = 3.0$ Å, $\Delta x = \Delta y = 1.0$ Å, and $L = 25$ Å. (b) Straight channel with variable pore radius. The pore radius tapers linearly from $R_p = 6.0$ Å at $i = 0$, to $R_p = 3.0$ Å near the channel center, and then increases linearly to $R_p = 5.0$ Å at $i = L/\Delta z - 1$, where $\Delta x = \Delta y = \Delta z = 1.0$ Å and $L = 35$ Å.

eq 16, and (iv) the Coulombic interaction in a uniform medium with ϵ_w. The results were obtained for the case where one ion is fixed at the channel center and a second ion is moved along the channel centerline in increments of 1.0 Å. The channel dimensions are $L = 25$ Å and $R_p = 2.0$ Å. For $r_{ij} < 2$ Å, Warshel et al.'s formula predicts a much larger ionic interaction than the effective potential in eq 16. Warshel et al.'s empirical formula includes the effect of dielectric variation around the ion due to the screening by the water and a much smaller dielectric constant $\epsilon_{eff} = 1$ is assumed in the ion center. Consequently, Warshel et al.'s formula gives a much larger ion−ion interaction when r_{ij} is very small. However, because the radii of the ions involved in permeation through protein channels are greater than ca. 1 Å, values of r_{ij} less than ca. 2 Å are inaccessible, or equivalently, only the regime where Warshel et al.'s effective potential is lower than the one proposed here is sampled during DLMC simulations (cf. section IV). For completeness, we show in Figure 7 the results of calculations using our model with $\epsilon_m = 2$, 5, and 10. Indeed, increasing ϵ_m reduces the repulsion between two like-charged ions in the pore. It is heartening to note that our effective ion−ion potential nicely reproduces the results of exact electrostatic calculations for *any* reasonable values of the system dielectric constants, and thus can be applied to cases where the input values of these constants are refined via additional microscopic or semimicroscopic considerations.

Effect of Channel Curvature. In addition to the simple cylindrical channel, we also tested the applicability of eq 16 for two types of channels with geometries that are more complicated than the simple cylindrical motif featured in the calculations presented above, namely, (i) a channel with a fixed pore radius but a curved channel centerline and (ii) a channel with a straight centerline but variable channel radius along the permeation axis. These channel geometries are depicted in Figure 8. For such cases where the channel structure changes smoothly along the permeation pathway, the proposed empirical formula with $c = 2.0$ describes the ion pair interaction to a high degree of accuracy. Panels a and b of Figure 9 show the ion−ion interaction in a channel with curved centerline: the channel radius is fixed at $R_p = 3.0$ Å. In Figure 9a, one ion is fixed at the channel center and a second ion is then moved along the centerline through the channel. In Figure 9b, one ion is fixed near the channel inlet while a second ion is moved along the channel centerline. The results obtained via our empirical approach are in good agreement with those based on the GNKC algorithm. Figure 10 shows the corresponding ion−ion interactions in a straight channel with variable channel radius. The agreement between the two computational approaches is again excellent.

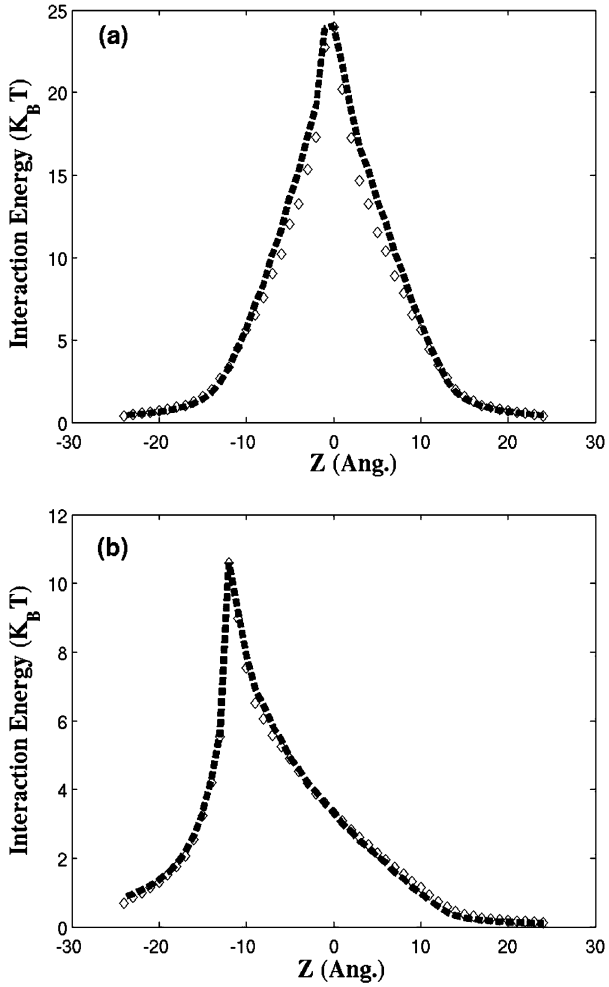

Figure 9. Ion−ion interaction in a channel with a curved centerline (see caption to Figure 8a for precise geometrical details): (a) one ion is fixed at the channel center and (b) one ion is fixed near the channel inlet. In both panels, a second ion is moved along the channel centerline in the z direction at internal increments of 0.1 nm. The dashed line presents results of numerical evaluation based on the GNKC procedure and the diamonds show results of the empirical formula eq 16 with $c = 2.0$.

IV. Dynamic Lattice Monte Carlo (DLMC) Simulations

We have performed dynamic lattice Monte Carlo (DLMC) simulations to test the empirical ion−ion interaction formula eq 16. A detailed description of the DLMC algorithm can be found in GNKC.[1,2] Here we give only a brief review. In the DLMC approach, configurations are generated by random changes of the ion positions. The total number of ions is characterized by $N = N_L + N_R + N_I + N_v$. Here N_L and N_R are the fixed numbers of ions on the left and right boundaries, which

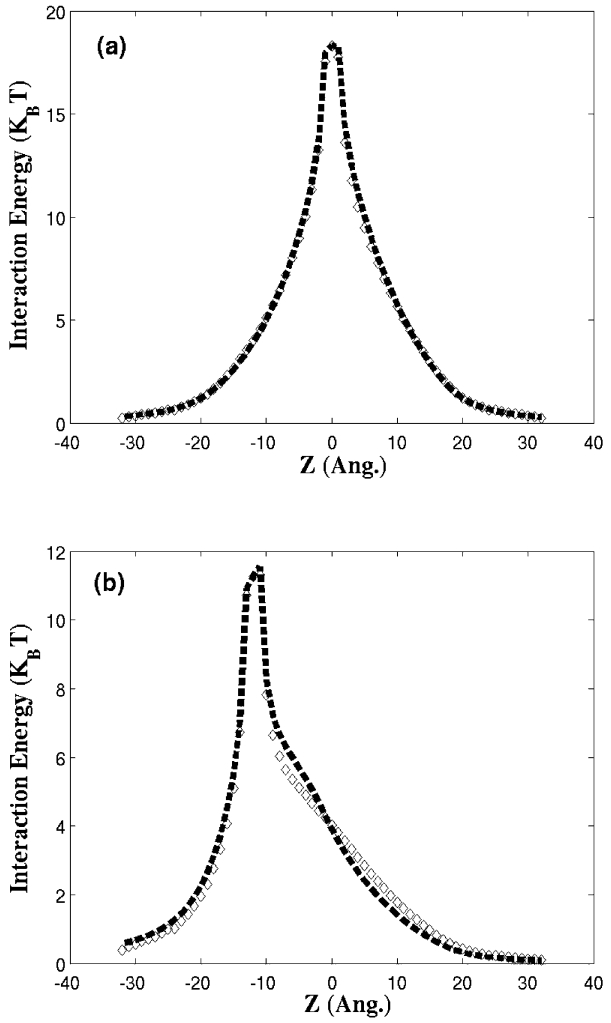

Figure 10. Ion−ion interaction in a straight channel with variable channel radius (see caption to Figure 8b for precise geometrical details): (a) one ion is fixed at the channel center and (b) one ion is fixed the channel inlet. In both panels, a second ion is moved along the channel centerline in the *z* direction at internal increments of 0.1 nm. The dashed line is the result of numerical evaluation based on the GNKC procedure, while the diamonds show the empirical formula eq 16 with $c = 2.0$.

are obtained by integrating the given boundary concentrations C_L and C_R over the volumes of the boundary layers. N_I is the number of ions inside the system and N_v is the number of virtual ions. The total number of ions N is fixed and N_I fluctuates. N_v is introduced only for counting purposes and is included to account for dynamic fluctuation of the number of ions in the interior of the system, and ensure the proportionality of Monte Carlo cycles to real time (characterizing time evolution under the corresponding multi-ion Smoluchowski equation). One Monte Carlo cycle consists of N steps. At each step, one ion is randomly chosen to move ±1 lattice point in one direction (x, y, or z), if the chosen ion is not a virtual one. This new configuration is accepted if Rand $< 1/(1 + \exp[\beta\Delta W])$, where Rand is a random number in the interval [0, 1] and $\beta = (k_B T)^{-1}$; ΔW is the energy change between the two configurations (see below for details). The total simulation time T_s is related to the number of Monte Carlo cycles N_c by:

$$T_s = \frac{h^2 N_c}{12D} \tag{18}$$

where h is the grid size and D is the diffusion coefficient for the ion. In a fully realistic model of permeation through a narrow ion channel, allowance should be made for the fact that the diffusion constant characterizing the motion of an ion inside the channel is different (lower, in general) than its bulk diffusion constant. However, the main goal of the present work is to ascertain the accuracy and efficiency of the effective potentials introduced in Section III, which can be done via a one-diffusion constant model. Hence, for simplicity, we adopt such a model for the kinetics calculations presented in this section.

The energy change based on the chosen particle k is

$$\Delta W = W_k^{new} - W_k^{old} \tag{19}$$

with

$$W_k = q_k\phi^{stat} + q_k{}^2\phi_k^{self} + \sum_{j\neq k}\frac{q_k q_j}{\epsilon_w}\phi^{coul}(r_{kj}) + \sum_{j\neq k} q_k q_j \phi_{kj}^{diel} \tag{20}$$

Here $q_k\phi^{stat}$ is the electrostatic energy of ion k: ϕ^{stat} can be obtained by solving Poisson's equation:

$$\nabla\cdot[\epsilon\nabla\phi^{stat}] = -4\pi\rho \tag{21}$$

based on the complete dielectric constant profile and the specified boundary potential (corresponding to an electrical potential difference $\Delta\phi$ across the left and right boundaries connected by a periodic electrical potential on the other four faces). Furthermore, ρ is the charge density due to the permanent charges in the protein. In the model considered in this paper, two cylindrical shells of charge are wrapped around the cylindrical pore. On the inner shell (pore lining), a total charge of Q is distributed uniformly on the lattice sites which satisfy $R_p < r \leq R_1$. On the outer shell, a total charge of $-Q$ is distributed uniformly on the lattice sites which satisfy $R_1 < r \leq R_2$. The permanent charge density at a given lattice site can be estimated as $\rho = \delta q/V_h$, where V_h is the volume of a lattice site, and δq is the amount of permanent charge on the lattice site. In the simulations described below, we used the following parameters: $Q = -1.5$ e, where e is the proton charge. For $R_p = 4.0$ Å, $R_1 = 5.0$ Å and $R_2 = 6.0$ Å; for $R_p = 8.0$ Å, $R_1 = 9.0$ Å and $R_2 = 10.4$ Å; and for $R_p = 12.0$ Å, $R_1 = 13.6$ Å and $R_2 = 15.0$ Å. Note that the permanent charge distribution on the protein adopted here renders the channel cation selective.

The dynamic Monte Carlo simulations presented in Figures 11−14 below were performed on a $65 \times 65 \times 33$ cubic lattice, with $h = 2$ Å and $a = 1.0$ Å$_c$, $r_c = 64$ Å. In these calculations the diffusion constant was taken to be $D = 10^{-5}$ cm^2/s. Periodic boundary conditions were applied to the x and y directions, while for the z direction the imposed concentrations were implemented with $C_L = C_R = 0.1$ M. For each conformational change that results in a change of the boundary concentration, one ion is randomly added to or removed from the boundary to keep a constant boundary concentration of 0.1 M. In contrast to the original implementation of the GNKC algorithm, the configurational energy change is calculated based on the chosen ion k as $\Delta W = W_k^{new} - W_k^{old}$, which does not distinguish an ion at a system boundary from one in the interior (the ion−ion interaction is calculated including ions at the boundaries). [This modification of the algorithm affects the way in which certain finite size simulation box artifacts are eliminated, as discussed in detail below.] We also imposed a hard-core excluded volume potential between any two mobile ions and between an ion and the membrane. In particular, we did not permit overlap between

mobile ions or between an ion and the protein/membrane. If an attempted move gave rise to this type of overlap, it was rejected.

On-the-fly calculation of all ion−ion interactions is not practical because repeated numerical solution of the Poisson equation during each Monte Carlo cycle is time consuming. Precalculating and storing the interaction between two ions at all possible pairs of lattice sites stretches the limits of computational and memory resources. Following the procedure established in GNKC, we divide the overall simulation system into two different regions (cf. Figure 1). For an ion in region I, the full dielectric constant profile is used and the values of the interaction potential with a second ion at all other positions are stored. In the present study, the self-energy of an ion inside region I is calculated and stored in coordinates (r, z) instead of (x, y, z), which saves 60−80% of the time needed to set up the self-energy lookup table utilized in the procedure outlined in GNKC. For two ions in region II, the system is simplified as a planar slab of membrane with thickness L and uniform dielectric constant ϵ_m bounded on two sides by regions of dielectric constant ϵ_w. Due to the high symmetry of the simplified bath|slab|bath system, the self-energy can be calculated and stored as a function of the ion's z coordinate only. Similar simplifications result for the ion−ion interaction. Given the z position of ion i, its interaction potential with another ion j depends only on $\vec{r}_j - \vec{r}_i \equiv \delta\vec{r}_{ji}$, and, therefore, for each value of z, the ion−ion interaction needs to be computed only as a function of one set of lattice points (to accommodate the entire range of $\delta\vec{r}_{ji}$). These simplifications significantly reduce the memory requirements for storing the precalculated interaction energy values, with increasing benefits as the size of region II increases.

In GNKC,[1] the DLMC update procedure described above is augmented by two additional steps, which are designed to correct for errors arising from the finite size of the simulation box. These are (1) image response to the average charge distribution and (2) boundary effects on ion screening energies. The first of these concerns the desire to prevent the (polarized) steady-state concentration distributions of ± ions from altering the externally imposed electric potential on the simulation box boundaries. This is a relatively minor effect (cf. Figure 6 of ref 1). Thus, we neglected it in the calculations presented here.

The second effect proved to be more substantial in the original implementation of GNKC (cf. Figure 5 of ref 1). Specifically, an ion in the aqueous region at the very edges of the simulation box is "deprived" of part of its immediate ionic atmosphere or screening shell (which, physically, is outside of the region covered by the simulation box, and therefore is not represented in the numerical calculation). Thus the simulation procedure artificially generates a destabilization penalty for ions that approach the boundaries of the simulation box. This penalty is of course artificial, and should be removed. In GNKC, a self-consistent procedure was implemented. First an equilibrium simulation is run in a "liquid junction" system (homogeneous aqueous medium with no membrane or channel). In the course of this simulation, the average electric potential energy (based on the Coulomb potentials produced by all ions in the system) is calculated, both for cations and anions, as a function of z. Because of the simulation artifact noted above, this potential (which is the same for both ± ions) is not "flat"—instead it increases near the boundaries of the simulation box. A correction potential energy, which accounts for the observed destabilization penalty, is obtained as the negative of the average electric potential energy profile just computed, added to the single-particle potential energy experienced by all ions, and then a new DLMC simulation is performed. From the configurations sampled by the new simulation, a new correction potential is calculated, appended to the single particle potential energy term, and the simulation is run again. This procedure is repeated until self-consistency is achieved. We have found that the need for this rather elaborate correction procedure can be eliminated simply by changing the configurational energy prescription as indicated above. In particular, by including the Coulomb interaction due to other ions in the boundary layer, we confer nearly the full effect of ionic screening of the test ion by nearby ions in its environment (effectively avoiding the removal of part of the solvent/electrolyte shell around the ion).

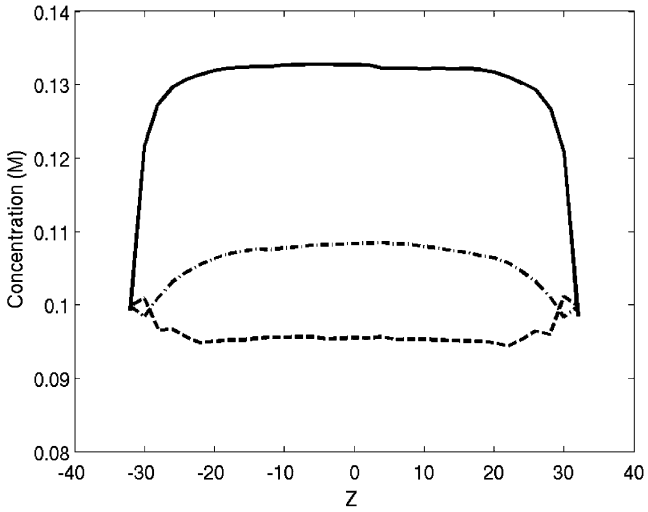

Figure 11. Salt concentration profile in an equilibrium system simulated without (solid line) ionic screening correction, with (dashed line) ionic screening correction based on the original GNKC algorithm, and using the dynamical update procedure introduced in the present study (dot dashed line).

To illustrate these issues, we consider in Figure 11 a system with a univalent binary salt for which the concentration boundary conditions were set, as noted above, to $C_L = C_R = 0.1$ M. (This is the same system addressed in Figure 5 of ref 1.) An exact procedure for calculating the steady-state concentration profiles in the interior of this system should give uniform equilibrium concentration profiles $C = 0.1$ M for both ion types. Our implementation incurs an 8% "swelling" of the concentration in the interior, whereas with the full ionic screening correction procedure in GNKC, the profile "shrinks" by 5%. Thus the errors are about the same for the two methods, and both represent a large improvement over the original GNKC procedure with*out* the corresponding ionic screening correction. The modification to GNKC introduced here thus represents a simplification of the procedure without any essential sacrifice in accuracy.[32]

Figure 12 compares cation and anion concentration profiles along the z-direction for a cylindrical channel with $L = 26$ Å, $R_p = 4.0$ Å, and an applied voltage of $\Delta\phi = \phi_L - \phi_R = 300$ mV, as calculated via DLMC simulation. The results presented here were averaged over eight individual simulation runs. Each concentration profile in the figure is actually a probability distribution, which was obtained by counting the number of particles in a cylindrical volume element of radius R_p and thickness h, and comparing this with the corresponding number density obtained at the boundaries.

The ion−ion interactions were calculated three different ways: (i) a Coulombic interaction with a uniform dielectric constant $\epsilon_w = 80$, (ii) eq 16 with $c = 2.0$, and (iii) numerically, using the GNKC approach. Similar concentration profiles were

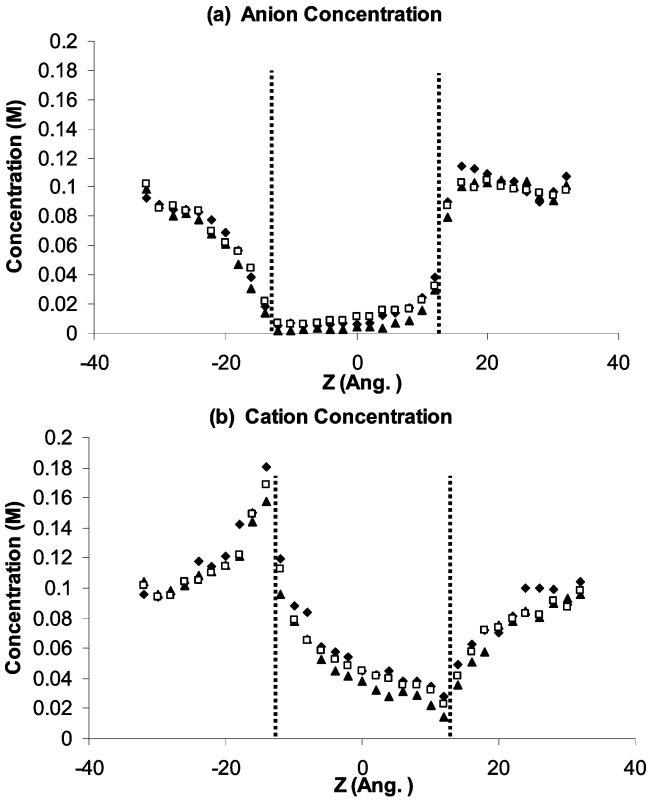

Figure 12. Steady-state concentration profiles along the z direction for a cylindrical channel with $R_p = 4.0$ Å and $L = 26$ Å at applied voltage $\Delta\phi = \phi_L - \phi_R = 300$ mV obtained via DLMC simulation: (a) concentration of anions and (b) concentration of cations. The ion−ion interactions were calculated three different ways: (i) a Coulombic interaction with a uniform dielectric field $\epsilon_w = 80$ (filled triangles), (ii) eq 16 with $c = 2.0$ (filled diamonds), and (iii) numerically, using the GNKC approach (open squares). The two vertical dotted lines mark the positions of the channel openings.

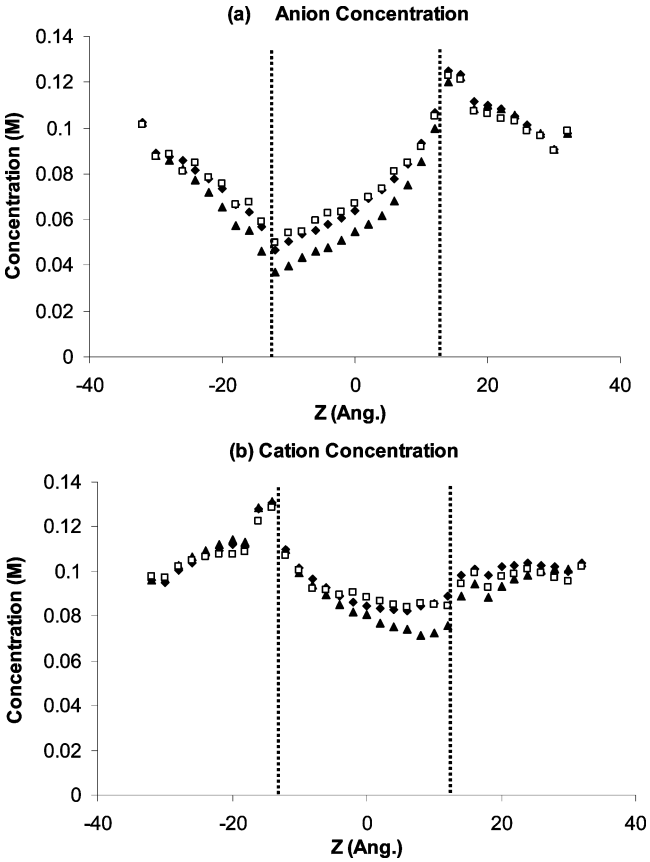

Figure 13. Steady-state concentration profiles along the z direction for a cylindrical channel with $R_p = 8.0$ Å and $L = 26$ Å at applied voltage $\Delta\phi = \phi_L - \phi_R = 300$ mV obtained via DLMC simulation: (a) concentration of anions and (b) concentration of cations. The ion−ion interactions were calculated three different ways: (i) a Coulombic interaction with a uniform dielectric field $\epsilon_w = 80$ (filled triangles), (ii) eq 16 with $c = 2.0$ (filled diamonds), and (iii) numerically, using the GNKC approach (open squares). The two vertical dotted lines mark the positions of channel openings.

obtained via all three procedures. For $R_p = 4.0$ Å, the probability of finding any ions inside the channel is only 3.5% (i.e., in 96.5% of the simulation time steps, the channel is empty). Thus, for this small channel radius, the dielectric contribution to the ion−ion interaction is relatively insignificant compared with other effects.

Figure 13 compares the concentration profile along the z direction for a cylindrical channel with $L = 26$ Å, $R_p = 8.0$ Å, and an applied voltage of $\Delta\phi = \phi_L - \phi_R = 300$ mV. For $R_p = 8.0$ Å, the possibility of finding one or more ions in the channel is close to 30%. As a result, the effect of the dielectric contribution to the ion−ion interaction is nonnegligible. Generally, the importance of the dielectric contribution to the ion−ion interaction increases with the ion concentration inside the channel. Similar effects (not shown here) were observed for $R_p = 12$ Å. The increase in the internal ion concentration (compared to calculations carried out with a uniform dielectric background characterized by ϵ_w) arises because the dielectric contribution ϕ_{ij}^{diel} generates a stronger attractive interaction between ions of different types.

Figure 14 compares the current−voltage curves obtained by the various methods for the channel radius $R_p = 8.0$ Å. The results presented here were again averaged over eight individual runs and the ion−ion interaction was calculated three different ways (vide supra). Our empirical formula eq 16 gives a current−voltage relation that is in reasonable agreement with that obtained from the GNKC algorithm. Including the dielectric contribution to the ion−ion interaction increases the flow rate for anions (by almost 10% for 300 mV). The effect of the dielectric contribution to the cation flow rate is less significant. The cation flow rate is always lower when the dielectric contribution is excluded. The dielectric contribution to the ion−ion interaction is not particularly pronounced in the model channel studied in this paper. However, in a recent study of the ion permeation in a glycine receptor channel (GlyR), where two strong binding sites exist near the entrance of the channel, we find that a large difference in the current−voltage curve is obtained when the dielectric contribution to the ion−ion interaction is neglected.[33]

V. Conclusions

The dielectric contribution to the ion−ion pair potential depends strongly on the positions of the two ions relative to the dielectric boundary. We have developed an efficient way to calculate the ion−ion interaction potential in a cylindrical channel. Furthermore, we find that the same empirical formula accurately describes ion transport for more complicated and biologically realistic channels, namely, (i) a "straight" channel with a radius that varies along the channel axis and (ii) a "curved" channel with fixed radius. This strongly suggests that we can use the method to study biologically relevant channels, e.g., the KcSA channel,[11] ClC channel,[12] acetylcholine,[13] and glycine receptor channels,[34] all of which are well-described by some combination of the geometric models considered in this

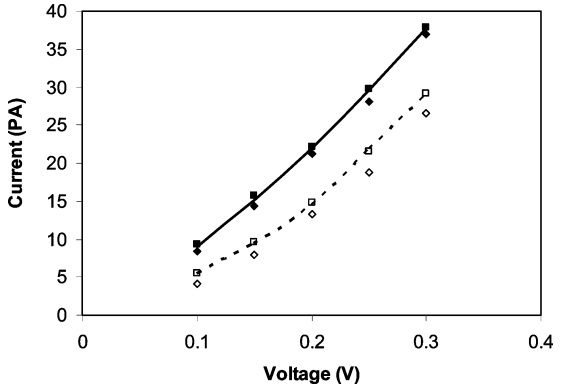

Figure 14. Current−voltage curves obtained from DLMC simulations for a cylindrical channel having $R_p = 8.0$ Å and $L = 26$ Å. The solid line shows cation current obtained via the GNKC algorithm, the filled squares show cation current based on the empirical formula of eq 16 with $c = 2.0$, and the filled diamonds show cation current based on Coulombic interaction in a uniform medium with ϵ_w. The dashed line shows anion current based on the GNKC algorithm, the open squares show anion current based on the empirical formula of eq 16 with $c = 2.0$, and the open diamonds show anion current based on Coulombic interaction in uniform medium with ϵ_w. Data points from all six $I-V$ curves are characterized by a standard deviation of ca. 3% for $\Delta\phi = 300$ mV and close to 15% for $\Delta\phi = 50$ mV; these error bars are suppressed in the plot for the sake of visual clarity.

study. The efficiency and accuracy of our empirical ion−ion pair potential was checked by using the dynamic lattice Monte Carlo (DLMC) simulation technique of Graf, Nitzan, Kurnikova, and Coalson (GNKC).[1] The concentration profiles and the current−voltage curves obtained with the empirical potential are in excellent agreement with the exact electrostatic calculations based on the algorithm of GNKC.

Use of the effective potentials developed in this work in DLMC (or, more generally, Brownian dynamics) simulations of ion permeation results in a significant speed-up relative to numerically exact evaluation of the relevant ionic forces, in particular with respect to (1) CPU requirements and (2) memory requirements.

(1) CPU requirements: In the GNKC algorithm, the evaluation of the DSE requires a separate set of Poisson calculations from those needed to calculate the ion−ion pair interactions. This is because a smeared out lattice charge is used to represent the charge on an ion when calculating the DSE, while a simple point charge representation is used when computing the dielectric contribution to the ion−ion pair potential. Using the effective ion−ion pair potential in eq 16 eliminates the need for the latter set of calculations, which are time-consuming (several days on a Pentium IV 3.0 GHz workstation).

(2) Memory requirements: After all of the Poisson equation solutions required for (1) have been carried out, exact numerical evaluation of the ion−ion pair potential requires a very large look-up table. [If there are N_L lattice points in the primary simulation region (i.e., not counting those that are so far out in the bulk that simplifying assumptions can be made to treat them) and N_M total number of lattice points in the simulation system, then there are roughly $N_L N_M$ pairs of ions for which the dielectric contribution to the ion−ion pair potential must be stored. For the system treated in Figure 8a, $N_L \approx 1200$, $N_M \approx (135)^3$.] This look-up table does not have to be constructed when our effective ion−ion potential is utilized: the formulas are simple enough that evaluation can be done "on the fly".

In addition, our investigations of the (single particle) DSE term showed that at least for the approximately cylindrical channel geometries studied here it is very well approximated by simple functional forms, identified above. Thus, even the relatively laborious DSE calculations may in principle be substantially simplified (provided that the DSE is evaluated exactly at a restricted set of positions in order to calibrate the DSE approximation formulas). Finally, these effective potentials are naturally suited for off-lattice Brownian dynamics simulations (where the force on each ion must be calculated at arbitrary points in 3D space), which provides additional flexibility (e.g., if the protein is allowed to dynamically fluctuate in the simulation).

Acknowledgment. Financial support from the National Science Foundation, the National Institutes of Health, and the Army Research Office is gratefully acknowledged.

References and Notes

(1) Graf, P.; Nitzan, A.; Kurnikova, M. G.; Coalson, R. D. *J. Phys. Chem. B* **2000**, *104*, 12324.
(2) Graf, P.; Kurnikova, M. G.; Coalson, R. D.; Nitzan A. *J. Phys. Chem. B* **2004**, *108*, 2006.
(3) Jordan, P. *Biol. Chem.* **1981**, *13*, 203.
(4) Levitt, D. G. *Biophys. J.* **1978**, *22*, 209.
(5) Jordan, P. *Biophys. J.* **1982**, *39*, 157.
(6) Åqvist, J.; Warshel A. *Biophys. J.* **1989**, *56*, 171.
(7) Mamonov, A.; Coalson, R. D.; Nitzan, A.; Kurnikova, M. G. *Biophys. J.* **2003**, *84*, 3646.
(8) Allen, T. W.; Anderson, O. S.; Roux B. *Proc. Nat. Acad. Sci. U.S.A.* **2004**, *101*, 117.
(9) Roux, B.; Karplus M. *J. Am. Chem. Soc*. **1993**, *115*, 3250.
(10) Jordan, P. *Biophys. J.* **1990**, *58*, 1133.
(11) Doyle, D. A.; Cabral, J. M.; Pfuetzner, R. A.; Gulbis, J. M.; Cohen, S. L.; Chait, B. T.; Mackinnon R. *Science* **1998**, *280*, 69.
(12) Dutzler, R.; Campbell, E. B.; Cadene, M.; Chait, B. T.; MacKinnon, R. *Nature* **2002**, *415*, 287.
(13) Miyazawa, A.; Fujiyoshi, Y.; Unwin, N. *Nature* **2003** *423*, 949.
(14) Kurnikova, M. G.; Coalson, R. D.; Graf, P.; Nitzan, A. *Biophys. J.* **1999**, *76* 642.
(15) Gardenas, A. E.; Coalson, R. D.; Kurnikova, M. G. *Biophys. J.* **2000**, *79*, 80.
(16) Eisenberg, R. S. *J. Membr. Biol*. **1996**, *150*, 1.
(17) Eisenberg, R. S. *J. Membr. Biol.* **1999** *171*, 1.
(18) Chung, S. H.; Allen, T. W.; Hoyles, M.; Kuyucak S. *Biophys. J.* **1999**, *77*, 2517.
(19) Corry, B. S.; Kuyucak, S.; Chung, S. H. *Biophys. J*. **2000**, *78*, 2364.
(20) Im, W.; Seefield, S.; Roux, B. *Biophys. J.* **2000**, *79*, 788.
(21) Mashl, R. J.; Tang Y. Z.; Schnitzer, J.; Jakobsson, E. *Biophys. J.* **2001**, *81*, 2473.
(22) Burykin, A.; Schutz, C.; Jilla, J.; Warshel, A. *Proteins*: *Struct., Funct., Genet.* **2002**, *47*, 265.
(23) Parsegian, A. *Nature* **1969**, *221*, 844.
(24) Klapper, I.; Hagstrom, R.; Fine, R.; Sharp, K.; Honig, B. *Proteins*: *Struct., Funct., Genet.* **1986**, *1*, 47.
(25) Press, W. H.; Flannery, B. P.; Teukolsky, S. A.; Vetterling, W. T. *Numerical Recipes in Fortran*: *The Art of Scientific Computing*; Cambridge University Press: Cambridge, 1992.
(26) Debye, P.; Pauling L. *J. Am. Chem. Soc*. **1925**, *47*, 2129.
(27) Warshel, A.; Russell, S. T.; Churg A. K. *Proc. Natl. Acad. Sci. U.S.A.* **1984**, *81*, 4785.
(28) Still, W. C.; Tempczyk, A.; Hawley, R. C.; Hendrickson T. *J. Am. Chem. Soc.* **1990**, *112*, 6127.
(29) Hassan, S.; Guarnieri, F.; Mehler, E. L. *J. Phys. Chem. B* **2000** *104*, 6478.
(30) Sham Y. Y.; Muegge I.; Warshel A. *Biophys. J.* **1998**, *74*, 1744.
(31) Schutz, C. N.; Warshel, A. *Proteins*: *Struct., Funct., Genet.* **2001**, *44*, 400.
(32) The $I-V$ curves presented in refs 1 and 2 were recalculated with the variation of the algorithm presented in this work. Currents obtained with the present version are consistently 10−20% larger than those obtained in the original implementation, since our ion screening correction slightly exaggerates the concentration in the system while the procedure used in GNKC slightly suppresses it, as is clear from Figure 11.
(33) Cheng, M. H.; Coalson, R. D.; Cascio M. Work in progress.
(34) Tang, P.; Mandal, P. K.; Xu Y. *Biophys. J.* **2002**, *83*, 252.